Rautiainen, Miina; Lukes, Petr

Spectral contribution of understory to forest reflectance in a boreal site

Published in:
Remote Sensing of Environment

DOI:
10.1016/j.rse.2015.10.009

Published: 15/12/2015

Document Version
Publisher's PDF, also known as Version of record

Remote Sensing of Environment 171 (2015) 98–104

Contents lists available at ScienceDirect

Remote Sensing of Environment

journal homepage: www.elsevier.com/locate/rse

Spectral contribution of understory to forest reflectance in a boreal site: an analysis of EO-1 Hyperion data

Miina Rautiainen [a,b,c,*], Petr Lukeš [d]

[a] Department of Forest Sciences, PO BOX 27, FI-10014 University of Helsinki, Finland
[b] Aalto University, School of Engineering, Department of Real Estate, Planning and Geoinformatics, PO Box 15800, 00076 Aalto, Finland
[c] Aalto University, School of Electrical Engineering, Department of Radio Science and Engineering, PO Box 13000, 00076 Aalto, Finland
[d] Global Change Research Centre, Academy of Sciences of the Czech Republic, Bělidla 4a, CZ-60300 Brno, Czech Republic

ARTICLE INFO

Article history:
Received 9 July 2015
Received in revised form 28 September 2015
Accepted 21 October 2015
Available online 27 October 2015

Keywords:
Forest reflectance model
Hyperspectral
Boreal
Leaf area index
Understory

ABSTRACT

Boreal forests exhibit strong seasonal dynamics in their reflectance spectra during the short, snow-free growing period. This short communication paper reports an analysis of the seasonality of boreal forest spectra from the end of snowmelt until the time of maximal leaf area. We apply a forest reflectance model (FRT) to estimate the seasonal contribution of understory vegetation to forest reflectance from a time series of three Earth Observing 1 (EO-1) Hyperion images acquired in May, June and July. The reflectance simulations are based on detailed seasonal series of leaf area index and understory spectra measurements carried out in ten stands at the Hyytiälä Forestry Field Station in Finland. Our results show that the contribution of understory to boreal forest reflectance is high in the visible domain, but it drops at the red edge and stays relatively low and constant in near infrared (NIR). Throughout the growing season, the contribution of the understory remains approximately the same in the NIR domain, whereas larger changes can be observed in the visible domain.

1. Introduction

Boreal forests exhibit strong seasonal dynamics in their reflectance spectra during their short, snow-free growing period. In the Eurasian boreal zone, connections between phenological events and seasonal reflectance courses have mainly been established for data from multispectral satellite sensors (Böttcher et al., 2014, Heiskanen et al., 2012, Jönsson, Eklundh, Hellström, Bärring, & Jönsson, 2010, Rautiainen, Nilson, & Lükk, 2009, Karlsen et al. 2008, Kobayashi, Suzuki, & Kobayashi, 2007), whereas studies based on seasonal time series of hyperspectral satellite images are nearly non-existent (Heiskanen, Rautiainen, Stenberg, Mõttus, & Vesanto, 2013). As new hyperspectral satellite missions (e.g. Environmental Mapping and Analysis Programme, EnMAP) are currently being developed, an understanding of the seasonality of vegetation spectra at a higher spectral resolution and beyond the most commonly applied vegetation indices is needed.

In boreal coniferous forests, the seasonal changes taking place in canopy structure (i.e. leaf area index, LAI) are small compared to broadleaved stands (Heiskanen et al., 2012, Rautiainen, Heiskanen, & Korhonen, 2012), and thus, changes in tree leaf and understory spectral compositions (Nikopensius, Pisek, & Raabe, 2015, Rautiainen et al., 2011, Miller et al., 1997) can be expected to be central driving factors of the spectral changes observed in a seasonal series of satellite images over a forest area. The needle turnover rate in northern European forests has significant latitudinal variation in the number of needle cohorts. For example, in Finland, Scots pine needle cohorts range from approximately 2 in the south to over 5 in the north, whereas for Norway spruce, the number of needle cohorts starts from 4 in the south and reaches up to 14 in the northernmost latitudes (Ťupek et al., 2015). In other words, the natural development of canopy structure is slow, and changes in understory spectral properties can therefore be expected to be a central driving factor of forest reflectance seasonality. Managed forests in northern Europe also tend to be sparse, and the forest floor is highly visible to satellite sensors (Eriksson, Eklundh, Kuusk, & Nilson, 2006). Therefore, potential differences in both the timing and magnitude of the seasonal reflectance cycles of the understory and overstory canopy layers also pose difficulties in the development of high spatial resolution global phenology products (e.g. Ganguly, Friedl, Tan, Zhang, & Verma, 2010) for northern forests.

Radiative transfer models offer a useful tool for analyzing the role of different components, such as understory vegetation, in forming forest reflectance as the growing season progresses. However, often the applicability of these models has been limited by the lack of seasonal series of field measurements needed as input variables (Nilson, Rautiainen, Pisek, & Peterson, 2012). In this paper, we report an analysis of the seasonality of boreal forest spectra from the end of snowmelt until the time of maximal leaf area. We apply a forest reflectance model to estimate

* Corresponding author at: Aalto University, School of Engineering, Department of Real Estate, Planning and Geoinformatics, PO Box 15800, 00076 Aalto, Finland.
E-mail address: miina.a.rautiainen@aalto.fi (M. Rautiainen).

http://dx.doi.org/10.1016/j.rse.2015.10.009

Table 1
A summary of study stands.

	Coniferous	Broadleaved
Number of stands	3 pine, 3 spruce	4 birch
Stand density (trees/ha)	1020–2520	920–2360
Mean tree height (m)	7.5–18.6	13.8–19.1
Mean diameter-at-breast-height (cm)	8.8–25.1	12–16.3
LAI_{eff} (May)	1.36–3.53	0.72–1.38
LAI_{eff} (June)	1.39–3.84	2.05–2.73
LAI_{eff} (July)	1.77–3.91	2.58–3.37

the seasonal contribution of understory vegetation to forest reflectance from a time series of Earth Observing 1 (EO-1) Hyperion images. Our analysis is based on a detailed seasonal series of canopy leaf area index, understory spectra and forest inventory measurements carried out at the Hyytiälä Forestry Field Station in Finland.

2. Materials and methods

2.1. Study site

Our study site, Hyytiälä, is located in southern boreal Finland (61° 50′ N, 24° 17′ E) and is mainly covered by Norway spruce (*Picea abies*), Scots pine (*Pinus sylvestris*) and Silver birch (*Betula pendula*) forests.

This study is based on data collected in 2010. No snow was observed in the study site after April 26, and based on traditional phenological observations (MetINFO, 2010), the first birch leaves emerged in mid-May (May 14–17) and reached their maximal size by early June (June 1–6) in the region around our study site. The height growth of Scots pines started in mid-May (May 13-16) and was completed by early July (July 6–9). The temperature sum for 2010 (growing degree days, GDD with a threshold of +5°C) was 1414 degree days (d.d.).

Ten monospecific stands from the Hyytiälä forest area were selected for our analysis (Table 1). The stands represented different age classes and species (Norway spruce, Scots pine, Silver birch) that are typical in the southern boreal forests. A stand inventory (using relascope sampling) was performed to obtain ancillary data on forest structure.

2.2. Field measurements

Seasonal courses of two dynamic variables influencing boreal forest reflectance, canopy LAI and understory spectra, were measured during 2010 (Table 2). The field campaign began in early May after snow had melted from the forest. Each stand was remeasured at approximately two-week intervals until October.

LAI for all ten study stands was measured with the LAI-2000 PCA instrument manufactured by LI-COR Inc. The sampling scheme was a cross with 12 measurement points: two perpendicular 6-point transects with 4-meter intervals between the measurement points. Two LAI-2000 units were used simultaneously. A reference sensor (sensor 'A') logged at 15-second intervals and was located above the forest canopy in a flux tower while the below canopy sensor (sensor 'B') was used to measure inside the forest. The forest measurements were made without view restrictors at a height of 0.7 m i.e. only tree canopies were included. All measurement points were marked with wooden sticks so that the exact same locations were used each time the measurements were repeated. To avoid sun flecks, the measurements were carried out during overcast sky conditions or, alternatively, in very early morning or late evening. The direct output of the instrument (effective leaf area index, here abbreviated as LAI_{eff}) is used in reporting our results.

Four stands, representing the different forest fertility site types in the Hyytiälä area, were chosen for measurements of understory spectra: 1) a xeric heath forest understory type covered by grey lichens and heather shrubs, 2) a sub-xeric heath forest understory type covered by mosses and sparse dwarf shrubs, 3) a mesic heath forest understory type covered by mosses and abundant dwarf shrubs, and 4) a herb-rich heath forest understory type covered by abundant herbaceous species and graminoids. The measurements were made in diffuse light conditions without fore-optics (i.e. the field-of-view was 25 degrees) with a FieldSpec Hand-Held UV/VNIR (325–1075 nm) Spectroradiometer manufactured by Analytical Spectral Devices (ASD). Three understory spectra per point were measured at intervals of 0.7 m on a 28-meter transect in each stand (i.e. 40 measurement points per transect were made). The ground area sampled at each point on the transect represented approximately the area of a circle with a radius of 25 cm. The data were processed to correspond to hemispherical-directional reflectance factors (HDRF). A detailed description of the measurements is provided by Rautiainen et al. (2011).

Table 3
A summary of EO-1 Hyperion images used in the study.

Date	View zenith angle (°)	Solar zenith angle (°)
5 May 2010	0.5	46.7
2 June 2010	14.8	41.5
3 July 2010	13.8	41.0

2.3. EO-1 Hyperion images

We used a three EO-1 Hyperion images from the Hyytiälä area in 2010: 5 May, 2 June and 3 July (Table 3). The series of images covers well the seasonal changes occurring in the forests: the early May image corresponds to the bud burst period for deciduous species, the early June image to the full leaf-out, and the early July image to time of maximal leaf area.

Hyperion is a narrowband imaging spectrometer, which has 242 spectral bands in the wavelength range from 356 to 2577 nm and a 30-m × 30-m spatial resolution (Pearlman et al., 2003). We used bands in the region from 488 to 1074 nm which corresponded to the spectral range of our field measurements. We began by downloading the Hyperion images as L1B products. First, we removed striping in the Hyperion images using spectral moment matching (Sun et al., 2008) and corrected for missing lines using local destriping (Goodenough et al., 2003). We also corrected for the spectral smile using interpolation and the pre-launch calibration measurements (Barry, 2001). Next, atmospheric correction was performed with the Fast Line-of-sight Atmospheric Analysis of Spectral Hypercubes (FLAASH) algorithm (Matthew et al., 2000). The aerosol levels were estimated using a ground-based optical weather sensor and atmospheric model by applying water levels obtained from measurements made by a sun photometer (AERONET network) in the image area. The atmospheric water levels were determined automatically by FLAASH using

Table 2
Time of data collection in 2010.

Time	Phenological stage (for broadleaved)	Dates of LAI measurements	Dates of understory measurements	Date of EO-1 Hyperion images	GDD[a] at the time of Hyperion acquisition
Early May	Budburst and leaf out	3–11 May	4–13 May	5 May	11
Early June	Full leaf out	26 May–7 June	31 May–9 June	2 June	218
Early July	Maximal leaf area	28 June–5 July	28 June–6 July	3 July	486

[a] GDD: growing degree days i.e. temperature sum with a threshold of +5 °C.

Table 4
Input variables in FRT simulations.

Input variable	Coniferous	Broadleaved	Reference
Shoot shading coefficient	0.59 (pine), 0.64 (spruce)	1	Calculated as 4 × STAR for pine and spruce according to Smolander et al. (1994) and Stenberg et al., (1995)
Shoot length, cm	15	40	
Specific leaf weight (g/m^2)	161 (pine), 202 (spruce)	57	Pine: Palmroth and Hari (2001), spruce: Stenberg et al., (1999), birch: Kull and Niinemets (1993)
Crown shape	Ellipsoid	Ellipsoid	Rautiainen et al. (2008b)
BAI/LAI ratio	0.18	0.15	Nilson (1999)

the spectral band centered at 1135 nm. The end product of the atmospheric correction process was hemispherical-directional reflectance factor (HDRF). Finally, we georeferenced the Hyperion images using approximately 20 ground control points (GCP) obtained from a digital topographic map and extracted mean HDRFs for each study stand using a 3 × 3 pixel (i.e. a 90-m × 90-m) window. The root mean square error (RMSE) for the GCPs was less than 0.5 pixels. The size of the pixel window corresponds approximately to the area covered by the field measurements (Section 2.2). More details on the preprocessing of this set of Hyperion images have previously been reported by Vesanto et al. 2012 and Heiskanen et al. 2013.

2.4. Forest reflectance simulations

A seasonal time series of spectra for the study stands was simulated with the FRT forest reflectance and transmittance model (Kuusk & Nilson, 2000) modified by Mõttus et al. (2007). FRT includes features of geometric-optical and radiative transfer equation based models. The model can simulate, for example, hemispherical-directional reflectance factors (HDRFs) for a forest stand in the wavelength range between 400 nm and 2400 nm. The FRT model is especially applicable in managed (i.e. relatively regular) forests for which commonly measured stand inventory data are available. It has previously shown good performance in boreal forests in both multiangular reflectance simulations (Rautiainen, Lang, et al. 2008) as well as in inversion mode (Rautiainen, 2005). The performance of this FRT version against other radiative transfer models has been documented in the RAMI exercises (Widlowski et al. 2007).

Stand structure is described by basic forest inventory variables: stand density, diameter at breast height and tree height. Forest variables that can be allometrically derived from the previous ones, e.g. crown length and radius, are also included. In addition, canopy density and structure are modeled using canopy leaf area index (LAI), needle clumping index and branch area index (BAI).

Stand HDRF (denoted by R) of a stand is calculated as:

$$R = R^1_{CR} + R^1_{GR} + R^{m+d} \quad (1)$$

where R^1_{GR} and R^1_{CR} and are the portions of the HDRF resulting from single scattering of direct radiation from the ground and tree crowns, respectively, and $R^{m+d}$is all multiply scattered direct radiation, and the reflectance (single and multiple scattering) of diffuse sky radiation. For a more detailed description on how the three components are calculated, the reader is referred to the original model description paper by Kuusk and Nilson (2000).

Input for the FRT simulations was based on the stand inventory data set and the seasonal leaf area index and understory spectral measurements described in Section 2.2. Leaf, needle and bark spectra, on the other hand, were based on other measurements available as open access data (Mõttus et al. 2014, Lukeš, Stenberg, Rautiainen, Mõttus, et al. 2013, Lang et al. 2002). A few input parameters had not been measured and thus, values from literature were used. These values and their sources are reported in Table 4. The selected stands were relatively even-aged, and therefore, trees in each stand were modeled as identical.

First, FRT was used to simulate the HDRFs in the wavelength range 488–1074 nm for each stand and for all three dates (May 5, June 2, July 3) corresponding to the viewing and illumination geometry of the Hyperion acquisitions (Table 3). The simulated HDRFs were compared to the HDRFs from Hyperion images. We chose for the comparison the HDRF simulated with FRT which corresponded to the mean wavelength of each Hyperion band. Next, we simulated the angular variation in HDRFs for all three dates assuming viewing angles from −70° to +70° at 5 degree intervals. The solar angles remained the same as in the Hyperion images. In all simulations, the contribution of understory vegetation to forest reflectance was calculated as R^1_{GR}/R.

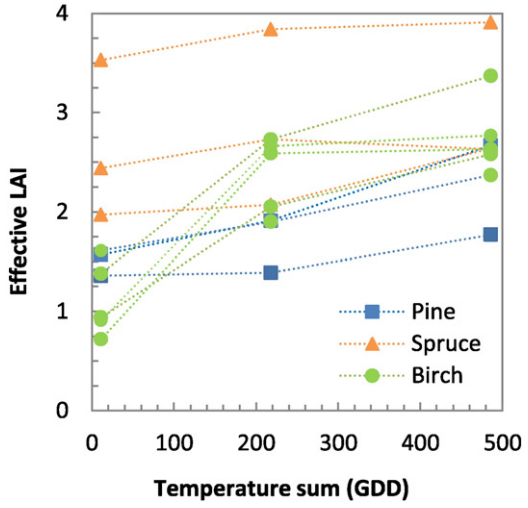

Fig. 1. Seasonal development of effective leaf area index (LAI_{eff}) in the study stands as a function of temperature sum (growing degree days, GDD, see Table 2). Please note that as the LAI_{eff} measurements were made with the LAI-2000 PCA instrument, the first values (made in the absence of foliage in early May) correspond to woody area index in the birch stands.

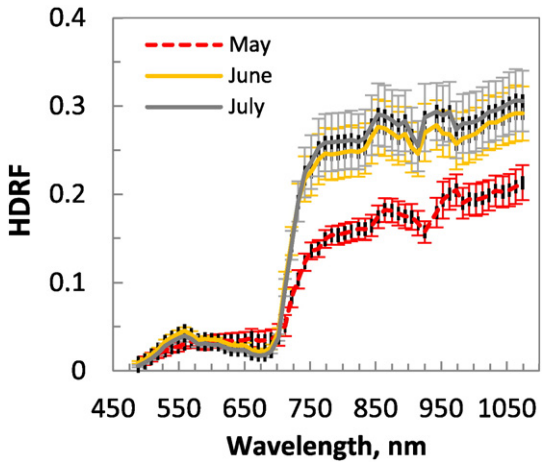

Fig. 2. The mean spectra of the ten study stands in early May, early June and early July obtained from EO-1 Hyperion images. The error bars show standard deviations.

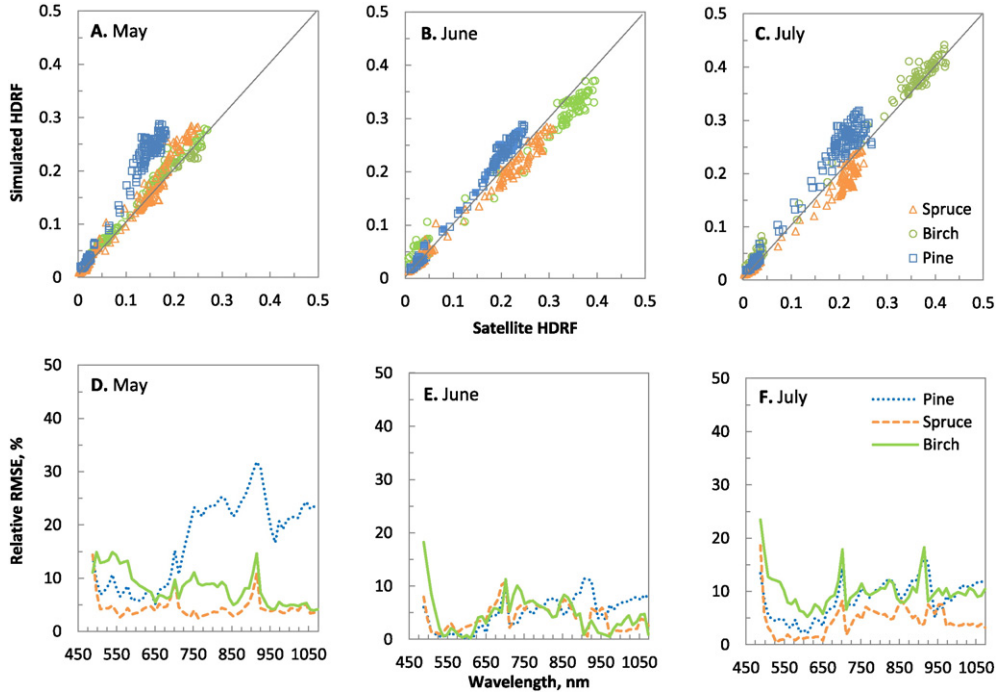

Fig. 3. A comparison of hemispherical-directional reflectance factors (HDRF, 488–1074 nm) from EO-1 Hyperion images and FRT simulations for all study stands in A. May, B. June and C. July. Relative root mean square errors (RMSE, in %) for the simulated and measured HDRFs in D. May, E. June and F. July.

3. Results and discussion

Between early May and early July, the forest canopies became more closed and the understory layer greener and more abundant. In the coniferous stands, due to growth of new annual shoots, the increase in LAI_{eff} was approximately 20%, whereas in the broadleaved stands, all leaves developed to their maximal size from buds (Fig. 1). The fractional cover of the upper understory vegetation increased on average from 0.06 to 0.2, and hence, the mean understory spectra also changed significantly. In early May, the understory spectra resembled a combination of litter (previous years' grasses and tree leaves) and green vegetation (mosses and multiannual dwarf shrubs). By early June, the understory vegetation went through green-up, and red edge features became steeper. A month later, in early July, the spectra of the studied understory types were clearly different, and also the within-site variations in understory spectra were the most notable. (Please see Rautiainen et al. 2011 for a more detailed discussion on the seasonality of the understory spectra for our study site.)

In the Hyperion images, the mean spectra of the study stands in May also clearly showed features of non-green vegetation (i.e. leafless birch trees and dead litter beneath the canopy): HDRFs in the red region were relatively high and in the NIR region relatively low (Fig. 2). Overall stand reflectance increased significantly during the month of May, and only marginally from early June to July. As previously reported by Heiskanen et al. (2013) for the same study area, the rapid changes in red and NIR (436–926 nm) stand reflectance can be linked to changes in canopy LAI and understory composition, and in SWIR (933–2406 nm) to the drying up of the forest floor after snow melt.

Overall, the FRT model performed slightly better in reflectance simulations during the summer months (June, July) than in the spring (May) (Fig. 3). For birch and spruce forests the simulations were relatively good from VIS to NIR wavelengths when compared to spectra obtained from the Hyperion images (relative RMSEs < 0.1). For pine stands, however, the difference between the measured and modeled NIR spectra was notably greater in spring (relative RMSE > 0.2). A potential explanation could be larger variation and/or rapid changes in pine needle optical properties in early phases of the growing season when compared to the other study species. The ratio of the abundance of new to old needles in canopies was not taken into account in the simulations due to the lack of in situ data, i.e. mean spectra for needle and leaf albedos were used. The large discrepancy between the measured and modeled reflectances in the blue region, on the other hand, can most likely be attributed to the poor calibration and low signal-to-noise ratio of the Hyperion sensor's blue bands, and/or residual errors of atmospheric correction, where Rayleigh scattering of atmospheric gases was not adequately accounted for.

A spruce and a birch stand were chosen to show in detail how forest reflectance was formed by understory and canopy components (Table 5). In these stands, FRT simulated spectra very similar to the ones obtained from Hyperion images for all three time periods (Fig. 4). The spectrum of the spruce stand changed only marginally during the growing period: the green region and NIR experienced small increases in stand reflectance. These changes can be linked to the emergence of new needles, small increase in LAI (<10%), and changes in the mesic understory spectrum. In the birch stand, where canopy LAI_{eff} nearly tripled during the study period, the red HDRFs decreased and NIR HDRFs increased notably. Also the shape of the R^1_{GR} (Eq. (1))

Table 5
Description of two study stands (in Fig. 4).

	Coniferous	Broadleaved
Species	Norway spruce	Silver birch
Stand density (trees/ha)	1114	2355
Mean tree height	15.2	14.1
Mean diameter-at-breast-height	18.9	12.0
LAI_{eff} (May, June, July)	2.44, 2.73, 2.63	0.91, 2.66, 2.77
Understory type	Mesic	Herb-rich
Fractional cover of upper understory layer (May, June, July)	0.04, 0.10, 0.13	0.06, 0.15, 0.18

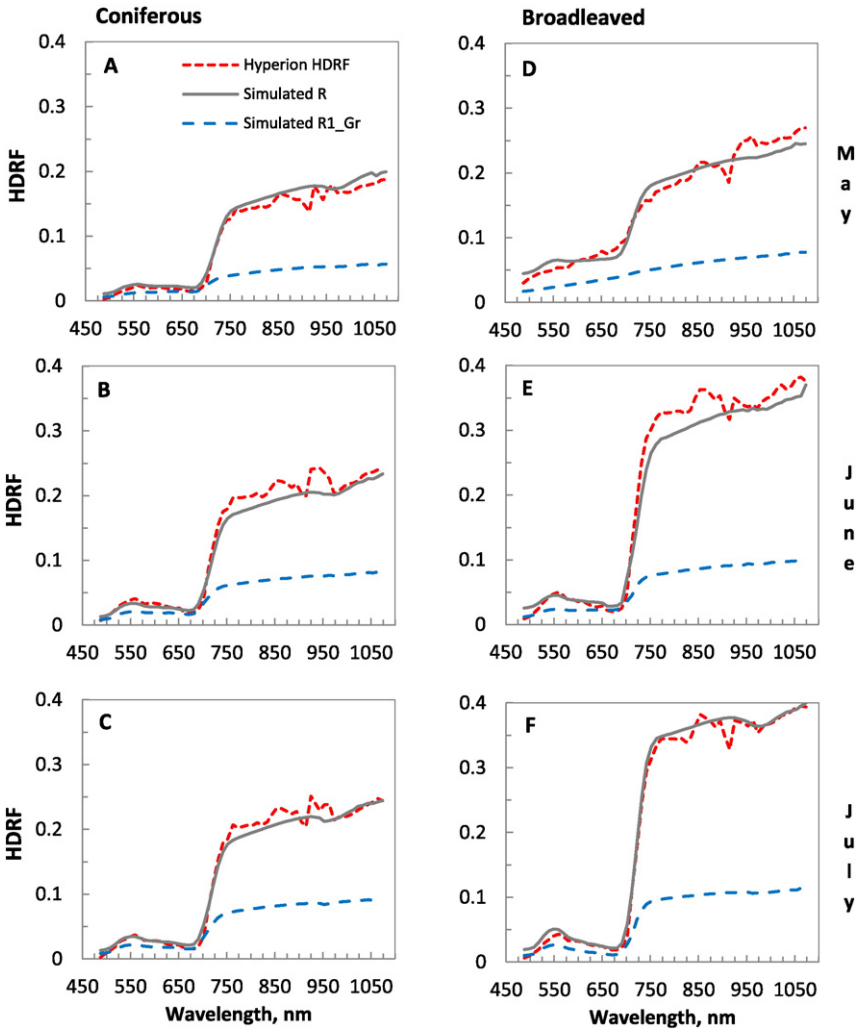

Fig. 4. A comparison of spectra from FRT simulations and EO-1 Hyperion images for a coniferous (A, B, C) and a broadleaved stand (D, E, F) in May (A, D), June (B, E) and July (C, F). The simulated forest reflectance curve shows R (i.e. $R = R^1_{CR} + R^1_{GR} + R^{m+d}$, Eq. (1)), and the simulated understory curve shows the component R^1_{GR}. For details on stand structure, see Table 3.

as a function of wavelength changed more in the birch than in the spruce stand.

Finally, the mean contribution of understory to forest reflectance was analyzed for all stands. In general, the highest contributions (>40%) were observed in the red range and the lowest (<30%) in the NIR region in close-to-nadir viewing angles (Fig. 5, 6). In the beginning of the growing season, there was considerable variation in the contribution in different VIS wavelengths (from 35 to 50%) due to the large contrast between the shape of the understory and tree leaf/needle spectra. As the growing season progressed, this variation flattened out. The contribution of understory to forest reflectance (in nadir) was constantly approximately 45% in the VIS and 25% in the NIR region. However, perhaps contrary to common assumptions, the contribution of understory to forest reflectance actually increased in many VIS wavelength regions between spring and summer. Even though the canopy LAI increased, the main gaps between (coniferous) trees remained the same and the understory spectra became significantly brighter (see Rautiainen et al. 2011) during the growing season. The contribution of understory strongly depended on the brightness ('site fertility type') of the understory.

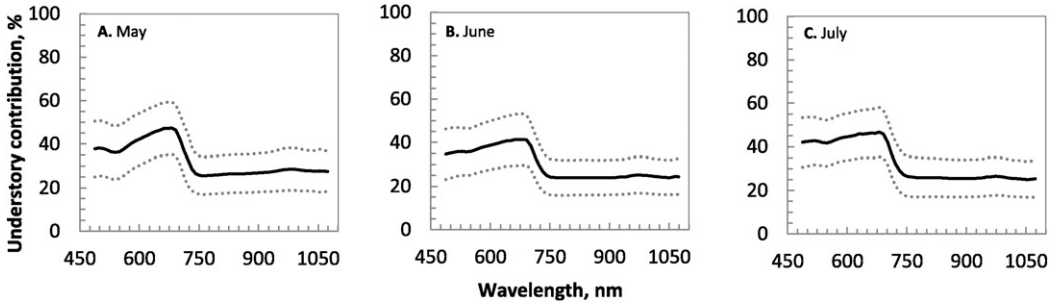

Fig. 5. The mean contribution of understory to stand reflectance (R^1_{GR}/R) as a function of wavelength from budburst to full leaf out for all study stands. A. In early May (mean LAI_{eff} 1.65). B. In early June (mean LAI_{eff} 2.46). C. In early July (mean LAI_{eff} 2.73). The black line shows the mean contribution and the gray dashed lines the standard deviations.

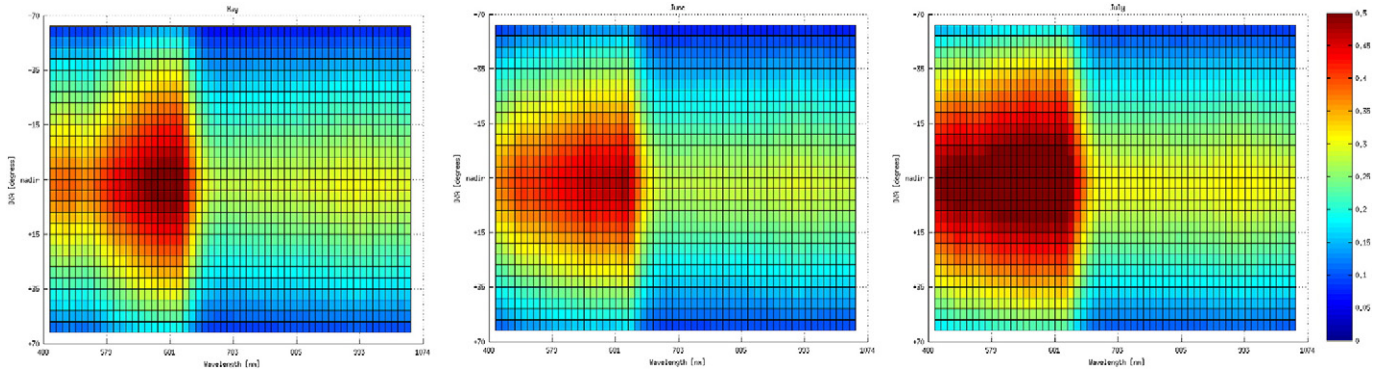

Fig. 6. The contribution of understory reflectance to total stand reflectance (R^1_{GR}/R) as a function of wavelength and observation zenith angle (OVA) in A. May, B. June and C. July. The values shown in the figure are averaged for all study stands. The color code on the right shows the level of understory contribution.

Several earlier papers have already reported that the understory has a key role in determining both the multispectral reflectance (e.g. Pisek et al. 2015, Rautiainen et al. 2007, Eriksson et al. 2006) and albedo (Lukeš, Stenberg, Rautiainen, 2013) of northern forests. This study extended the analysis to high-to-medium spatial resolution hyperspectral remote sensing data. Our results showed that the contribution of understory to forest reflectance in is high in the visible domain, but drops at the red edge and stays relatively low and constant in NIR. This is especially promising for retrieving canopy structure using new algorithms which apply, for example, the directional area scattering factor (DASF) calculated from the range between 710 and 790 nm (Vanhatalo, Rautiainen, Stenberg, 2014, Knyazikhin et al. 2012).

Acknowledgments

We thank Janne Heiskanen and Matti Mõttus for collaboration in the project, and Titta Majasalmi and Anu Akujärvi for field work. The study was funded by the Academy of Finland and Ministry of Education, Youth and Sports of CR within the National Sustainability Program I (NPU I), grant number LO1415.

References

Barry, P. (2001). *EO-1/Hyperion science data user's guide*. Defense & Information Systems, Redondo Beach: TRW Space.

Böttcher, K., Aurela, M., Kervinen, M., Markkanen, T., Mattila, O. -P., Kolari, P., ... Pulliainen, J. (2014). MODIS time-series-derived indicators for the beginning of the growing season in boreal coniferous forest — A comparison with CO_2 flux measurements and phenological observations in Finland. *Remote Sensing of Environment*, *140*, 625–638.

Eriksson, H., Eklundh, L., Kuusk, A., & Nilson, T. (2006). Impact of understory vegetation on forest canopy reflectance and remotely sensed LAI estimates. *Remote Sensing of Environment*, *103*, 408–418.

Ganguly, S., Friedl, M., Tan, B., Zhang, Z., & Verma, M. (2010). Land surface phenology from MODIS: Characterization of the Collection 5 global land cover dynamics product. *Remote Sensing of Environment*, *114*, 1805–1816.

Goodenough, D.G., Dyk, A., Niemann, K.O., Pearlman, J.S., Chen, H., Han, T., ... West, C. (2003). Processing Hyperion and ALI for forest classification. *IEEE Transactions on Geoscience and Remote Sensing*, *41*(6), 1321–1331.

Heiskanen, J., Rautiainen, M., Stenberg, P., Mõttus, M., & Vesanto, V. (2013). Sensitivity of narrowband indices to boreal forest LAI, reflectance seasonality and species composition. *ISPRS Journal of Photogrammetry and Remote Sensing*, *78*, 1–14.

Heiskanen, J., Rautiainen, M., Stenberg, P., Mõttus, M., Vesanto, V., Korhonen, L., & Majasalmi, T. (2012). Seasonal variation in MODIS LAI for a boreal forest area in Finland. *Remote Sensing of Environment*, *126*, 104–115.

Jönsson, A., Eklundh, L., Hellström, M., Bärring, L., & Jönsson, P. (2010). Annual changes in MODIS vegetation indices of Swedish coniferous forests in relation to snow dynamics and tree phenology. *Remote Sensing of Environment*, *114*, 2719–2730.

Karlsen, S. -R., Hogda, K., Wielgolaski, F., Tolvanen, A., Tomervik, H., Poikolainen, J., & Kubin, E. (2009). Growing-season trends in Fennoscandia 1986–2006 determined from satellite and phenology data. *Climate Research*, *39*, 275–286.

Knyazikhin, Y., Schull, M., Stenberg, P., Mõttus, M., Rautiainen, M., Yang, Y., ... Myneni, R. (2012). Hyperspectral remote sensing of foliar nitrogen content. *Proceedings of the National Academy of Sciences of the United States of America (PNAS)*www.pnas.org/cgi/doi/10.1073/pnas.1301247110

Kobayashi, H., Suzuki, R., & Kobayashi, S. (2007). Reflectance seasonality and its relation to the canopy leaf area index in an eastern Siberian larch forest: Multi-satellite data and radiative transfer analysis. *Remote Sensing of Environment*, *106*, 238–252.

Kull, O., & Niinemets, U. (1993). Variations in leaf morphometry and nitrogen concentration in *Betula pendula* Roth., *Corylus avellana* L. and *Lonicera xylosteum* L. *Tree Physiology:*, *12*(3), 311–318.

Kuusk, A., & Nilson, T. (2000). A directional multispectral forest reflectance model. *Remote Sensing of Environment*, *72*, 244–252.

Lang, M., Kuusk, A., Nilson, T., Lükk, T., Pehk, M., & Alm, G. (2002). *Reflectance spectra of ground vegetation in sub-boreal forests*http://www.aai.ee/bgf/ger2600/index.html

Lukeš, P., Stenberg, P., & Rautiainen, M. (2013a). Relationship between forest density and albedo in the boreal zone. *Ecological Modeling*, *261-262*, 74–79.

Lukeš, P., Stenberg, P., Rautiainen, M., Mõttus, M., & Vanhatalo, K.M. (2013b). Optical properties of leaves and needles for boreal tree species in Europe. *Remote Sensing Letters*, *4*(7), 667–676.

Matthew, M.W., Adler-Golden, S.M., Berk, A., Richtsmeier, S.C., Levine, R.Y., Bernstein, L.S., ... Miller, D.P. (2000). Status of atmospheric correction using a MODTRAN4-based algorithm. *Proc. SPIE*, *4049*, 199.

MetINFO, 2010. URL: http://www.metla.fi/metinfo/fenologia. Accessed 23 February 2015.

Miller, J.R., White, H.P., Chen, J.M., Peddle, D.R., McDermid, G., Fournier, R.A., ... LeDrew, E. (1997). Seasonal change in the understory reflectance of boreal forests and influence on canopy vegetation indices. *Journal of Geophysical Research*, *102*(D24), 29475–29482.

Mõttus, M., Stenberg, P., & Rautiainen, M. (2007). Photon recollision probability in heterogeneous forest canopies: compatibility with a hybrid GO-model. *Journal of Geophysical Research*, *112*, D03104http://dx.doi.org/10.1029/2006JD007445.

Mõttus, M., Sulev, M., & Hallik, L. (2014). Seasonal course of the spectral properties of alder and birch leaves. *IEEE Journal of Selected Topics in Applied Earth Observations and Remote Sensing.*, *7*(6), 2496–2505.

Nikopensius, M., Pisek, J., & Raabe, K. (2015). Spectral reflectance patterns and seasonal dynamics of common understory types in three mature hemi-boreal forests. *International Journal of Applied Earth Observation and Geoinformation* in press.

Nilson, T. (1999). Inversion of gap frequency data in forest stands. *Agricultural and Forest Meteorology*, *98-99*, 437–448.

Nilson, T., Rautiainen, M., Pisek, J. & Peterson, U. 2012. Chapter 3: Seasonal reflectance courses of forests. In (Ed. A. Oteng-Amoako): New advances and contributions to forestry research (ISBN 979-953-307-503-6), InTech, pp. 34-58.

Palmroth, S., & Hari, P. (2001). Evaluation of the importance of acclimation of needle structure, photosynthesis, and the respiration to available photosynthetically active radiation in Scots pine canopy. *Canadian Journal of Forest Research*, *31*(7), 1235–1243.

Pearlman, J.S., Barry, P.S., Segal, C.C., Shepanski, J., Beiso, D., & Carman, S.L. (2003). Hyperion, a space-based imaging spectrometer. *IEEE Transactions on Geoscience and Remote Sensing*, *41*(6), 1160–1173.

Pisek, J., Rautiainen, M., Nikopensius, M., & Raabe, K. (2015). Estimation of seasonal dynamics of understory NDVI in northern forests using MODIS BRDF data: semi-empirical versus physically-based approach. *Remote Sensing of Environment*, *163*, 42–47.

Rautiainen, M. (2005). Retrieval of leaf area index for a coniferous forest by inverting a forest reflectance model. *Remote Sensing of Environment*, *99*, 295–303.

Rautiainen, M., Heiskanen, J., & Korhonen, L. (2012). Seasonal changes in canopy leaf area index of a boreal forest site in central Finland. *Boreal Environmental Research*, *17*(1), 72–84.

Rautiainen, M., Suomalainen, J., Mõttus, M., Stenberg, P., Voipio, P., Peltoniemi, J., & Manninen, T. (2007). Coupling forest canopy and understory reflectance in the Arctic latitudes of Finland. *Remote Sensing of Environment*, *110*, 332–343.

Rautiainen, M., Lang, M., Mõttus, M., Kuusk, A., Nilson, T., Kuusk, J., & Lükk, T. (2008a). Multiangular reflectance properties of a hemiboreal forest: an analysis using CHRIS PROBA data. *Remote Sensing of Environment*, *112*, 2627–2642.

Rautiainen, M., Mõttus, M., Heiskanen, J., Akujärvi, A., Majasalmi, T., & Stenberg, P. (2011). Seasonal reflectance dynamics of common understory types in a northern European boreal forest. *Remote Sensing of Environment*, *115*(12), 3020–3028.

Rautiainen, M., Mõttus, M., & Stenberg, P. (2008b). Crown envelope shape measurements and models. *Silva Fennica*, *42*(1), 19–33.

Rautiainen, M., Nilson, T., & Lükk, T. (2009). Seasonal reflectance trends of hemiboreal birch forests. *Remote Sensing of Environment*, *113*, 805–815.

Smolander, H., Stenberg, P., & Linder, S. (1994). Dependence of light interception efficiency on structural parameters. *Tree Physiology*, *14*, 971–980.

Stenberg, P., Kangas, T., Smolander, H., & Linder, S. (1999). Shoot structure, canopy openness, and light interception in Norway spruce. *Plant, Cell and Environment*, *22*(9), 1133–1142.

Stenberg, P., Linder, S., & Smolander, H. (1995). Variation in the ratio of shoot silhouette area to needle area in fertilized and unfertilized Norway spruce trees. *Tree Physiology*, *15*(11), 705–712.

Sun, L., Neville, R., Staenz, K., & White, H.P. (2008). Automatic destriping of Hyperion imagery based on spectral moment matching. *Canadian Journal for Remote Sensing*, *34*(S1), S68–S81.

Ťupek, B., Mäkipää, R., Heikkinen, J., Peltoniemi, M., Ukonmaanaho, L., Hokkanen, T., ... Lehtonen, A. (2015). Foliar turnover rates in Finland — Comparing estimates from needle-cohort and litterfall-biomass methods. *Boreal Environment Research*, *20*, 283–304.

Vanhatalo, K., Rautiainen, M., & Stenberg, P. (2014). Monitoring the broadleaf fraction and canopy cover of boreal forests using spectral invariants. *Journal of Quantitative Spectroscopy and Radiative Transfer*, *133*, 482–488.

Vesanto, V., Mõttus, M., Heiskanen, J., Rautiainen, M., Majasalmi, T. 2012. Atmospheric correction of a seasonal time series of Hyperion EO-1 images and red edge inflection point calculation. Proceedings of the fourth workshop on hyperspectral remote sensing and signal processing: Evolution in remote sensing (June 4–7, 2012, Shanghai). IEEE Xplore: 4 p.

Widlowski, J. -L., Taberner, M., Pinty, B., Bruniquel-Pinel, V., Disney, M., Fernandes, R., ... Xie, D. (2007). The third RAdiation transfer Model Intercomparison (RAMI) exercise: Documenting progress in canopy reflectance modeling. *Journal of Geophysical Research*, *112*(D09111), 28. http://dx.doi.org/10.1029/2006JD007821.